J. Biochem. 128, 271–281 (2000)

NMR Studies of Model Peptides of PHGGGWGQ Repeats within the N-Terminus of Prion Proteins: A Loop Conformation with Histidine and Tryptophan in Close Proximity[1]

Hitoshi Yoshida,* Norio Matsushima,‡,2 Yasuhiro Kumaki,† Mitsuo Nakata,* and Kunio Hikichi*

**Division of Biological Sciences and †High-Resolution NMR Laboratory, Graduate School of Science, Hokkaido University, Kita-ku, Sapporo,Hokkaido 060-0810; and ‡School of Health Sciences, Sapporo Medical University, Chuo-ku, Sapporo, Hokkaido 060-8556*

Received April 13, 2000; accepted May 29, 2000

The N-terminal region of the prion protein from human and mouse contains five tandem repeats with the consensus sequence of PHGGGWGQ. NMR studies were performed in water for two cyclic peptides, cyclo-[$C^1R^2Q^3P^4H^5G^6G^7S^8W^9G^{10}Q^{11}R^{12}D^{13}C^{14}$] (C1) and cyclo-[$C^1R^2D^3P^4H^5G^6G^7G^8W^9G^{10}Q^{11}P^{12}H^{13}G^{14}G^{15}G^{16}W^{17}G^{18}Q^{19}R^{20}D^{21}C^{22}$] (C2), which are cyclized by a disulfide bridge between the Cys residues at the N- and C-termini, and for their corresponding linear peptides (L1 and L2) which are formed by reduction. The patterns of the $C_\alpha H$ chemical shift difference of these four peptide mimetics were very similar to those observed for the tandem repeats of human prion protein reported by other researchers. The medium-range NOE connectivities were found between the $C_\beta H$ of the H5 and the proton of the W9 side chain for L1. The corresponding NOEs were also observed in H5-W9 and H13-W17 of L2 with ambiguity. These observations indicate that histidine (i) is in close proximity to tryptophan (i+4). $d_{\alpha N}$ (i,i+2) NOE connectivities were observed between W9 and Q11 of L1 and L2, and d_{NN} (i,i+1) NOE connectivities were also observed for G10-Q11 of L1 and L2 and for G18-Q19 of L2. Significantly lower temperature coefficients of amide proton chemical shifts were obtained for Q11 and Q19 of L2 and C2. Structure calculations for L1 showed that HGG(G/S)W and (G/S)WGQ adopt a loop conformation and a β-turn, respectively. These results strongly suggest that the tandem repeats within prion protein adopt a non-random structure.

Key words: β-turn, histidine-tryptophan interaction, N-terminus, octapeptide repeat, prion protein.

The "prion hypothesis" holds that an aberrant conformation of a normal cellular protein is the essential, perhaps sole, component of infection agent responsible for several fatal neurodegenerative diseases, including bovine spongiform encephalopathy (BSE), sheep spongiform encephalopathy ("scrapie"), and the human genetic disease Creutzfeldt-Jakob disease (CJB) (*1*). Although it is not certain that the prion protein is their agent of these diseases, it is a primary component of infectious brain fractions, and infection occurs only in hosts expressing the prion protein. In the course of disease, the normal 20 kDa cellular prion protein (PrP^c) is converted into a form with modified secondary structure (PrP^{Sc}).

Little is known about the normal cellular role of the prion protein. Although no enzymatic activity is associated with the protein, both *in vivo* results with mammalian proteins (*2–4*) and studies of synthetic peptides (*5–8*) have shown that prion proteins can bind copper ions at an N-terminal site containing five tandem repeats of the octapeptide PHGGGWGQ (Fig. 1).

Recent NMR studies of full-length PrP revealed that the N-terminus including the tandem repeats is highly flexible, while the remainder adopts a globular shape (*9–11*). Sequential assignments of the tandem repeats were impossible because of overlapping resonances. Furthermore, the assignment of NOE connectivities and the value of $^3J_{HNH\alpha}$ were ambiguous. This situation has apparently hindered any detailed investigation of the structure of the tandem repeats within the prion protein. In contrast, spectroscopic data show that membrane binding of PrP results in a significant ordering of the N-terminal part of the molecule (*12*). Circular dichroism study suggested that a synthetic octapeptide repeat adopts a non-random, extended conformation with properties similar to the poly-L-proline type II left-handed helix (*13*). Raman spectroscopy suggested that the binding of copper to octapeptide PHGGGWGQ induces formation of an α-helical structure in the GWGQ segment (*7*). It appears that there are some discrepancies among these observations on the structure of the octapeptide repeats.

The aim of this study is to obtain more reliable informa-

[1] This work was supported in part by a Special Grand-in-Aid for Promotion of Education and Science in Hokkaido University provided by the Ministry of Education, Science, Sports, and Culture (to K.H.) and by a Grant-in-Aid for Scientific Research from the Ministry Education, Science, Sports and Culture of Japan (to N.M.).

[2] To whom correspondence should be addressed. Tel: +81-11-611-2111, Fax: +81-612-3617, E-mail: matusima@shs.sapmed.ac.jp

```
23  KKRPKPGGWNTGGSRYPGQGSPGGNRYP  50
51  PQGGGGWGQ                     59
60  PHGGGWGQ                      67
68  PHGGGWGQ                      75
76  PHGGGWGQ                      83
84  PHGGGWGQ                      91
92  GGGTHSQWNKPSKPKTNMKHMAGAAAAGAVVGG 124
```

Fig. 1. **Sequence of the flexible N-terminus of human prion (*59*).**

tion on the preferred structure of the tandem repeats of PHGGGWGQ. Here we performed NMR studies of cyclic and linear peptides containing one or two repeat units within the prion protein to obtain NMR parameters reflecting folded structure. The cyclic peptides may be less flexible and adopt more stable structure than linear peptides. Common structural features of all tandem repeat units in peptides with different repeat numbers (one and two) are likely to reflect a potential structure of tandem repeats in the prion protein. Cyclic peptides were successfully used in NMR studies to identify β-turns in YSPTSPS repeats of the CTD within RNA polymerase II (Kumaki *et al.*, unpublished results) and in PGQGQQ repeats of high molecular weight gluten proteins (*14*).

MATERIALS AND METHODS

Peptide Design—We designed the following cyclic peptides for this study.

C1: cyclo-[$C^1R^2Q^3P^4H^5G^6G^7S^8W^9G^{10}Q^{11}R^{12}D^{13}C^{14}$]

C2: cyclo-[$C^1R^2D^3P^4H^5G^6G^7G^8W^9G^{10}Q^{11}P^{12}H^{13}G^{14}G^{15}G^{16}$-$W^{17}G^{18}Q^{19}R^{20}D^{21}C^{22}$]

Cyclic peptides **C1** and **C2** contain one and two PHGG(G/S)WGQ repeats, repectively. The PHGGSWGQ segment is found in mouse prion protein. These peptides are cyclized through a disulfide bridge between the Cys residues at the N- and C-termini. Hydrophilic amino acids Arg and Asp are also introduced at both sides of the tandem repeat in order to enhance the solubility in water. These cyclic peptides were prepared by Science Tanaka (Ishikari).

The cyclic peptides (**C1** and **C2**) were reduced by adding 19–20 mM dithiothreitol (DTT) to yield the corresponding linear peptides (**L1** and **L2**).

L1: $C^1R^2Q^3P^4H^5G^6G^7S^8W^9G^{10}Q^{11}R^{12}D^{13}C^{14}$

L2: $C^1R^2D^3P^4H^5G^6G^7G^8W^9G^{10}Q^{11}P^{12}H^{13}G^{14}G^{15}G^{16}W^{17}G^{18}$-$Q^{19}R^{20}D^{21}C^{22}$

Complete reduction was achieved since the signals gave only one set for respective **L1** and **L2** after 12 h.

Sample Preparation—Purified peptides were dissolved in water containing 50 mM KCl and 0.02% sodium azide. **L1** and **C1** were completely dissolved without precipitation and thus dissolved at high concentration. The peptide concentrations of **L1** and **C1** were 6.7 and 7.9 mM, respectively, and the pH values were 6.6 and 6.2 in H_2O/D_2O (90%:10%), respectively. The solubility of **L2** and **C2** (especially **C2**) was not so high at this range of pH in spite of the introduction of hydrophilic amino acids. The peptide concentrations of **L2** and **C2** were less than 3.7 mM. Their pH values were 6.6 in H_2O/D_2O (90%:10%), respectively. Comparison of the 1D spectra obtained at two different concentrations of **L1** (0.2 and 7.9 mM) and of **L2** (0.2 and 3.7 mM) at 298 K indicated no concentration dependence of resonance. TSP was added to the solutions as an internal reference (0.0 ppm).

NMR Measurements—All NMR experiments were performed on a JEOL alpha 500 and 600 spectrometers, and the NMR data processing was done on a SGI O2 workstation using NMRPipe software. NMR experiments were performed at 278 K except for experiments of temperature coefficients of amide proton resonances. The temperature was maintained within ±0.1 K. The temperature dependence of the amide proton chemical shifts was determined from measurements at 278, 283, 293, 303, and 313 K for all peptides studied here.

NOESY experiments were also performed at 100, 200, 300, 400, 500, and 650 ms in order to assess NOE buildup profile for **L2**. The NOE buildup rates about cross-peaks within Trp ring indicated that the buildup is fairly linear from 100 to 400 ms. Sequence-specific assignments of proton resonance were obtained by 2D NOESY (mixing time = 300 ms), TOCSY (mixing time = 70 ms), and DQF-COSY experiments. Water signal was suppressed by DANTE presaturation. The $^3J_{HNH\alpha}$ coupling constants were also determined.

Structure Calculations—For **L1**, 38 unambiguously assigned NOE correlations were used to calculate structure. NOE cross-peaks corresponding to fixed distances between aromatic ring protons (Trp $C_{\varepsilon 3}H$-$C_{\zeta 3}H$) were used as internal standards. NOEs were assigned as strong, medium, weak, and very weak. Lower boundary limits were set at 1.8 Å for all NOEs, and upper boundary limits were set at 3.5 Å for strong, 4.5 Å for medium, 5.0 Å for weak, and 5.5 Å for very weak. The φ angle of His5 of which $^3J_{NH\alpha}$ coupling constants were >8 Hz was restricted to $-120 \pm 30°$. No hydrogen bonding restraints were used in any of the calculations.

Structures were calculated using the program X-PLOR version 3.851 (*15*). The standard files parallhdg.pro and topallhdg.pro were used to define the force constants and residue topologies, respectively. Random coordinate files were generated using generate_template.inp. One hundred substructure embedded coordinate files were generated using the dg_sub_embed.inp protocol (*16*, *17*). Distance geometry and simulated annealing were performed on the 100 subembedded structures using the dgsa.inp protocol (*16–18*). This protocol performs initial energy minimization using the conjugated gradient method, followed by 6,000 steps of restrained molecular dynamics at 2,000 K and 3,000 steps of simulated annealing to 100 K for a total of 33 ps of dynamics. These structures were then subjected to a final step of minimization. The resulting 100 coordinate files were refined using the protocol refine.inp. Dynamics were begun at 1,000 K and consisted of 2,000 cooling steps to 100 K for a total of 10 ps of simulated annealing. A final stage of minimization was performed using a repel value of 0.75 to define the VDW potential.

Using a cutoff of 0.1 Å for upper bound NOE violations and 5° for dihedral angle bound violations, 42 structures were left from the 100 refined structures. The 15 lowest energy structures were used to represent the final acceptable ensemble for **L1**.

RESULTS

NMR Resonance Assignments—Table I describes the amino acid assignments for the four peptide mimetics (**L1**, **L2**, **C1**, and **C2**) in H_2O/D_2O (90%:10%) at 278 K. Identification of their individual amino acid residues was completed unambiguously by TOCSY experiments (Fig. 2). Sequential assignment of the proton resonances for **L1** and **C1** was completed by sequential NOE connectivity $d_{\alpha N}(i,i+1)$ except for C1 or R2.

$C_\alpha H$ Chemical Shift Difference—$C_\alpha H$ chemical shifts are sensitive to peptide backbone conformation. The chemical shift deviations of $C_\alpha H$ resonance from random coil values

TABLE I. **Resonance assignments for two linear peptides (L1 and L2) and two cyclic peptides (C1 and C2).** [a] The chemical shifts for each amino acid at 278 K. The chemical shifts are reported in parts per million. [b] $^3J_{HNH\alpha}$ is three-bond scalar coupling between the backbone amide proton and the α proton. $^3J_{HNH\alpha}$ is reported in herz. [c] $-\Delta\delta/\Delta T$ is the temperature coefficient of the amide proton chemical shifts. The coefficients measured between 278 and 298 K are included ($-\Delta ppb/\Delta K$). [d] The chemical shifts of $C_{\varepsilon 2}H$ on Gln are 6.95/7.70 and 7.00/7.57 ppm. The number of residues was not determined because of overlapping. [e] The chemical shifts of ($C_{\delta 1}H$, $C_{\varepsilon 2}H$) on Trp are 6.95/7.70 and 7.00/7.57 ppm. The number of residues was not determined because of overlapping. [f] The chemical shifts of $C_{\varepsilon 2}H$ on Gln are 6.97/7.62 ppm and 6.96/7.68 ppm. The number of residues was not determined because of overlapping.

Residue	Chemical shift[a] HN	Hα	Hβ	Hγ	Other	$^3J_{HNH\alpha}$[b]	$-\Delta\delta/\Delta T$[c]
(a) L1 : CRQPHGGSWGQRDC							
C1	N D	4.06	2.97/3.05	-	-	N D	N D
R2	8.65	4.34	1.78/1.83	1.64	δ : 3.17/3.17, ε : 7.26	N D	9.60
Q3	8.72	4 59	1.89/2.06	2.37	ε2: 7.00/7 59	6.9	9.60
P4	-	4.34	1.78/2.17	1.94	δ : 3.62/3.74	-	-
H5	8.55	4.62	3.14/3.14	-	δ2: 7.07, ε1: 8.05	8.1	7 67
G6	8.54	3.97	-	-	-	-	6.90
G7	8.44	3.95	-	-	-	-	7.15
S8	8.36	4.47	3.80/3.80	-	-	7.9	7.46
W 9	8.38	4.66	3.28/3.33	-	δ1: 7.25, ε1· 10.18, ε3: 7 61, ζ2· 7.47, ζ3. 7.14, η2: 7.23	6.8	6.92
G10	8.40	3.77/3.86	-	-	-	-	6.18
Q11	8.22	4.31	1.97/2 11	2.33	ε2: 6.94/7.70	7.2	5.57
R12	8.50	4.37	1.78/1.87	1.62/1.62	δ : 3.16/3.16, ε : 7.22	7.7	6.71
D13	8.62	4.66	2.66/2.73	-	-	7.2	6.42
C14	7.97	4.37	2.94/2.94	-	-	7.2	5.11
(b) L2 : CRDPHGGGWGQPHGGGWGQRDC							
C1	N D	N D	N D	-	-	N D	N D
R2	N D	N D	N D	N D	δ : 3.09/3.09, ε : 7.19	N D	N D
D3	8.64	4.81	2.58/2.70	-	-	6.3	9.44
P4	-	4.31	1.73/2.14	1.92	δ : 3.75/3.83	-	-
H5	8.52	4 66	3.08/3.19	-	δ2: 7.04, ε1: 8.07	8.5	5.05
G6	8.21	3.97	-	-	-	-	3.51
G7	8.46	3.92	-	-	-	-	6.95
G8	8.41	3.87	-	-	-	-	7.21
W 9	8.20	4.59	3.23/3.30	-	δ1: 7.22, ε1: 10.17, ε3: 7.58, ζ2: 7.45, ζ3: 7.12, η2: 7.21	6.8	6.40
G10	8.44	3.75/3.80	-	-	-	-	6.57
Q11	8.09	4.53	1.83/2.02	2.28	ε2: 6.96/7.61	7.7	4.98
P12	-	4.27	1.73/2.12	1.91	δ : 3.58/3.71	-	-
H13	8.54	4.59	3.11/3.11	-	δ2: 7.04, ε1: 8.03	8.7	7.95
G14	8.52	3.95	-	-	-	-	7.08
G15	8.46	3.92	-	-	-	-	6.95
G16	8.39	3.87	-	-	-	-	6.15
W17	8.22	4.61	3.22/3.30	-	δ1: 7.22, ε1: 10.17, ε3: 7.58, ζ2: 7.45, ζ3: 7.12, η2: 7.21	6.8	6.36
G18	8.48	3.77/3.81	-	-	-	-	6.53
Q19	8.20	4.30	1.94/2.08	2.30	ε2: 6.94/7.69	7.4	5.19
R20	8.48	4.34	1.73/1.84	1.58/1.58	δ : 3.09/3.09, ε : 7.19	7.3	6.17
D21	8.60	4.64	2.64/2.73	-	-	7.8	N D
C22	7.96	4.37	2.92/2.92	-	-	7.8	4.69

(*19*) [$\Delta\delta C_\alpha H$ = $\delta C_\alpha H$ (observed) – $\delta C_\alpha H$ (random coil)], where the random coil value of Gln/Asp preceding Pro is corrected by taking account of nearest-neighbor effects (*20*), are shown in Fig. 3.

The main feature is that the $C_\alpha H$ resonance of G10 in all of the four peptide mimetics (**L1**, **L2**, **C1**, and **C2**) shows significantly larger upfield shifts than those of all other residues. The same is observed for G18 of **L2** and **C2**. Moreover, values of $\Delta\delta$ $C_\alpha H$ of P4 and H5 for the four peptide mimetics and of P12 and H13 of **L2** and **C2** are larger than those of the other residues except for G10 or G18. Such behaviors of $C_\alpha H$ chemical shift difference are very similar to those calculated from $C_\alpha H$ chemical shifts of the tandem repeats within human prion, as shown in Fig. 3c (*11*). This suggests that the peptide mimetics used here adopt a similar backbone conformation to that of the tandem repeats of human prion protein.

The chemical shifts of the two $C_\alpha H$ resonances for G10 and G18 are also different from each other (Fig. 3). Thus, their dihedral angles (ϕ, φ) are defined.

Identification of Cis/Trans Isomers of Gln-Pro Peptide Bonds—The peptide bond X-Pro (X means arbitrary residue), such as Gln-Pro seen in QPHGGGWGQ, has two distinct preferred conformations, *trans* and *cis* (*21–23*). *Cis-trans* isomerization is slow on the NMR time scale. Therefore, it is expected that X-Pro peptide bonds will give two sets of resonances corresponding the trans and cis isomers. The sequential $d_{\alpha\delta pro}$ (i,i+1) NOE connectivities, which are

TABLE I (continued)

Residue	Chemical shift[a] HN	Hα	Hβ	Hγ	Other	$^3J_{HNH\alpha}$[b]	$-\Delta\delta/\Delta T$[c]
(c) C1 : cyclo-[CRQPHGGSWGQRDC]							
C1	8.04	4.41	3.05	-	-	N D	5.63
R2	N D	N D	N D	N D	δ : 3.16/3.16, ε : 7.25	N D	N D
Q3	8.55	4.59	1.86/2.05	2.33	ε2:[d]	7.3	8.31
P4	-	4.31	1.75/2.14	1.92	δ : 3.62/3.70	-	-
H5	8.54	4.67	3.19	-	δ2: 7.16, ε1: 8.25	8.2	5.69
G6	8.52	3.94/4.00	-	-	-	-	5.53
G7	8.43	3.95	-	-	-	-	6.31
S8	8.36	4.47	3.80/3.80	-	-	7.3	6.68
W9	8.40	4.66	3.80/3.80	-	δ1: 7.25, ε1: 10.18, ε3: 7.61, ζ2: 7.48, ζ3: 7.15, η2: 7.23	6.4	6.47
G10	8.41	3.83/3.88	-	-	-	-	5.83
Q11	8.25	4.31	1.97/2.11	2.34	ε2:[d]	7.4	5.63
R12	8.48	4.34	1.75/1.84	1.61/1.61	δ : 3.13/3.13, ε 7.22	6.7	7.15
D13	8.53	4 67	2.61/2.72	-	-	7.3	5.53
C14	8.18	4.41	3.05/3.19	-	-	6.8	7.15
(d) C2 cyclo-[CRDPHGGGWGQPHGGGWGQRDC]							
C1	N D	N D	N D	-	-	N D	N D
R2	N D	N D	N D	N D	δ : 3.08, ε : 7.19	N D	
D3	8.61	4.81	2.58/2.73	-	-	7.5	8.43
P4	-	4.27	1 75/2.13	1.92	δ : 3.58/3.72	-	-
H5	8.54	4.67	3.08/3.25	-	δ2: 7.12, ε1: 8.20	8.2	3 47
G6	8.20	3.98	-	-	-	-	2.84
G7	8.46	3.94	-	-	-	-	6.91
G8	8.43	3.91	-	-	-	-	7.25
W9	8.25	4.59	3.23/3.30	-	δ1: •, ε1: •, ε3: 7.57, ζ2: 7.45, ζ3: 7.12, η2: 7.21	6.7	6.33
G10	8.48	3.77/3.83	-	-	-	-	6.51
Q11	8.07	4.56	1.84/2.05	2 30	ε2:[f]	7.8	4.58
P12	-	4.30	1.69/2.13	1.89	δ : 3.75/3.82	-	-
H13	8.55	4.63	3.13/3.13	-	δ2: 7.06, ε1: 8.10	8.8	8.92
G14	8.52	3.98	-	-	-	-	6.06
G15	8.46	3.94	-	-	-	-	6.91
G16	8.39	3.89	-	-	-	-	5.15
W17	8.24	4.61	3.23/3.30	-	δ1: •, ε1: •, ε3: 7.57, ζ2: 7.45, ζ3: 7.12, η2: 7.21	6.8	6.33
G18	8.54	3.80/3.84	-	-	-	-	6.46
Q19	8.16	4.33	1.94/2.09	2.30	ε2:[f]	6.8	3.80
R20	8.41	4.33	1.75/1.83	1 58/1.58	δ : 3.08, ε H: 7.19	7.3	4.88
D21	8.57	4.72	2.64/2.75	-	-	7.3	5.93
C22	8.20	4.45	3.03/3.31	-	-	7.8	7.16

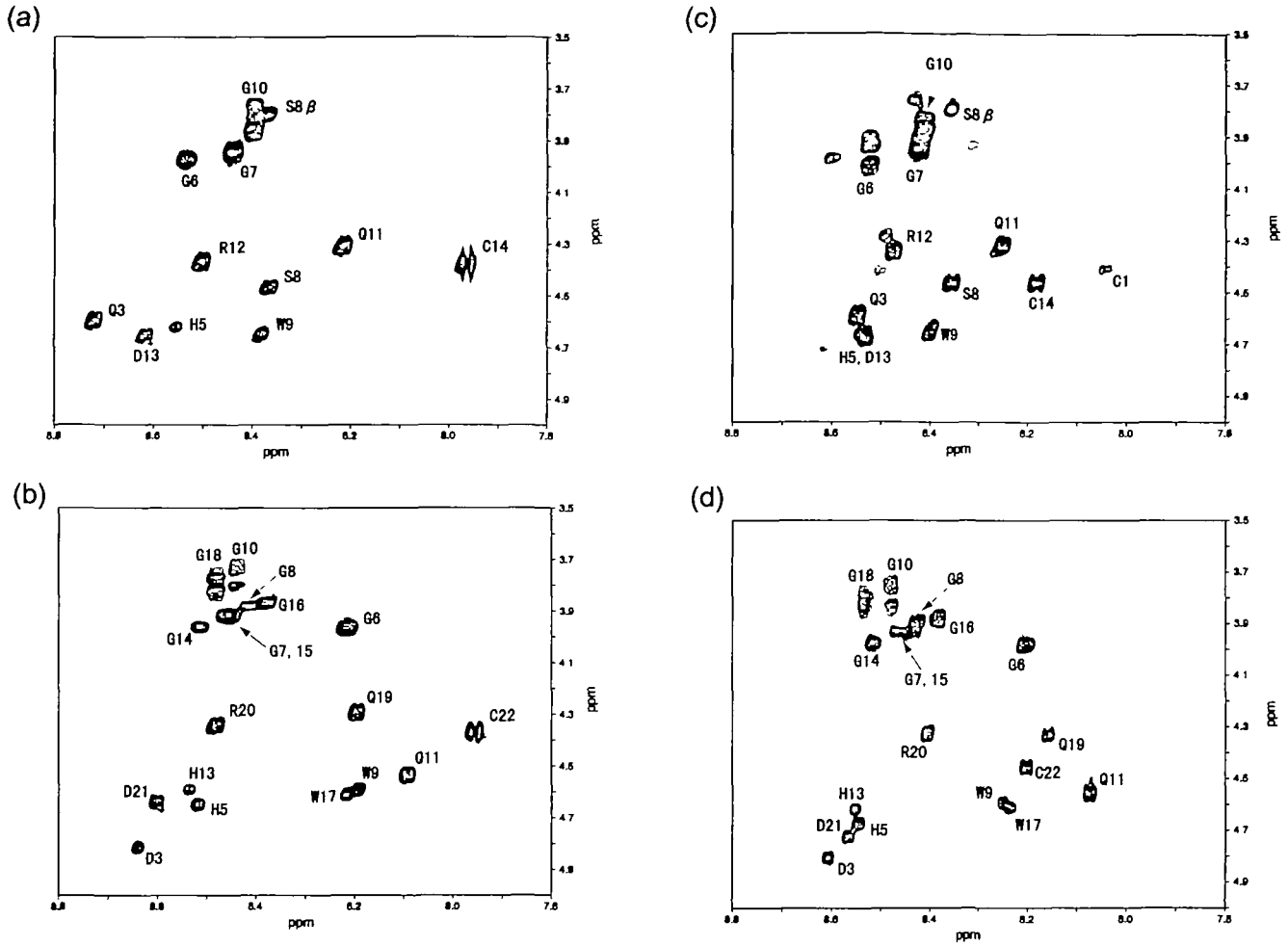

Fig. 2. **The fingerprint-regions of the TOCSY spectra of two linear peptides (L1 and L2) and two cyclic peptides (C1 and C2).** (a) **L1** ($C^1R^2Q^3P^4H^5G^6G^7S^8W^9G^{10}Q^{11}R^{12}D^{13}C^{14}$); (b) **L2** ($C^1R^2D^3P^4H^5G^6G^7G^8W^9G^{10}Q^{11}P^{12}H^{13}G^{14}G^{15}G^{16}W^{17}G^{18}Q^{19}R^{20}D^{21}C^{22}$); (c) **C1** (cyclo-[$C^1R^2Q^3P^4H^5G^6G^7S^8W^9G^{10}Q^{11}R^{12}D^{13}C^{14}$]); (d) **C2** (cyclo-[$C^1R^2D^3P^4H^5G^6G^7G^8W^9G^{10}Q^{11}P^{12}H^{13}G^{14}G^{15}G^{16}W^{17}G^{18}Q^{19}R^{20}D^{21}C^{22}$]). The TOCSY spectra were measured at 278 K. Each intraresidue spin system is connected by a solid line and annotated by standard one-letter symbol for the amino acid and residue number in the sequence.

expected for trans peptide bonds, were observed for the Gln-Pro segment (Q3-P4) of **L1** and the Asp-Pro (D3-P4) and Gln-Pro (Q11-P12) segments of **L2**. The $d_{\alpha\delta pro}$ $(i,i+1)$ NOE cross-peaks were also observed for the cyclic peptides (**C1** and **C2**). These NOEs indicate that Gln/Asp-Pro peptide bonds in the four peptide mimetics are all *trans*.

Vicinal Coupling Constants $^3J_{HNH\alpha}$—The $^3J_{HNH\alpha}$ coupling constant for each residue of the four peptidemimetics is given in Table I. We find that the $^3J_{HNH\alpha}$ values of H5 in **L1**, **L2**, and **C1**, and of H13 of **L2** are significantly larger than 8.0. This indicates that the ϕ angles of these His are defined.

NOE Connectivities—We found NOE cross-peaks between the protons of tryptophan side chain and the $C_\beta H$ of histidine side chain; there are medium-range NOE connectivities (Fig. 4, a, b, and c). For **L1**, NOEs are observed between H5 and W9 (**1**, **2**, and **3** in Fig. 4a). These cross-peaks are not W9-R12 NOE, as indicated in Fig. 4b. **L2** has cross-peaks at corresponding positions to those observed for **L1** (**1**, **2**, **3**, **4**, **5**, and **6** in Fig. 4c). It is likely that the cross-peaks (**1**, **2**, and **3** in Fig. 4c) are attributable to H5-W9 NOE.

Moreover, there are NOE cross-peaks between the protons of tryptophan or histidine side chains and the α-proton of glycine. For **L1**, G6/G7-W9 NOE and G6/G7-H5 NOE are observed (**4**, **5**, and **6** in Fig. 4a). It is likely that, for **L2**, there are G7-W9 NOE and G15-W17 NOE (**4**, **5**, and **6** in Fig. 4c) with ambiguity.

Further, there are NOE cross-peaks between the protons of the tryptophan aromatic ring and the α-protons of other residues. S8-W9 NOE and W9-G10 NOE were observed for **L1** without ambiguity. For **L2**, G8-W9 NOE, W9-G10 NOE, G16-W17 NOE, and W17-G18 NOE were observed with ambiguity. The W9-Q11 NOE was observed for **L1** and W17-Q19 for **L2**.

NMR Parameters Reflecting a β-Turn Structure—The following three NMR parameters are considered to be a diagnostic tool of a β-turn conformation: (a) The d_{NN} (3,4) NOE connectivity is observed (*24*). A weak $d_{\alpha N}$ (2,4) NOE may be also observed (*24*). The d_{NN} (2,3) connectivity is expected for type I β-turns and the strong $d_{\alpha N}$ (2,3) connectivity for the type II turns (*24*). (b) The temperature coefficient of the

amide proton chemical shift ($-\Delta\delta/\Delta T$) of the residue at position 4 is less than 4.5–5.3 ppbK^{-1} (*25–33*). (c) The α protons of a β-turn are in general shifted upfield (*30*, *31*). Using these criteria, we examined the NMR data obtained for the four peptide mimetics in water.

(a) NOE connectivities: The $d_{\alpha N}(i,i+2)$ NOE connectivities were observed between W9 and Q11 for **L1** and **L2** without ambiguity (Fig. 5), while they were not observed for **C1** and were unclear for **C2**. The $d_{\alpha N}$ $(i,i+2)$ NOE connectivities between W17 and Q19 of **L2** were unclear because of an overlapping peak. The d_{NN} $(i,i+1)$ NOE connectivities were observed between G10 and Q11 for **L1**, **C1**, and **L2**, while **C2** did not show such an NOE. The d_{NN} $(i,i+1)$ NOE connectivities were observed between G18 and Q19 for **L2** and **C2**. These NOEs are expected for a β-turn at G/SWGQ.

(b) Temperature coefficients of the amide proton chemical shifts: The temperature coefficients of the amide proton chemical shifts ($-\Delta\delta/\Delta T$) for each residue of the four peptide mimetics (**L1**, **L2** and **C1** and **C2**) are given in Table I. Remarkable reduction in $-\Delta\delta/\Delta T$ is observed for Q11 and Q19 for **C2**. Such significantly lower temperature coefficients are also observed for Q11 and Q19 in the corresponding linear peptide (**L2**). The low temperature coefficients for the above Gln residues are indicative of hydrogen bonding and are compatible with those at position 4 in a β-turn. The present results support the presence of a β-turn at GWGQ in each unit of **L2** and **C2**.

(c) $C_\alpha H$ chemical shift difference: As noted, all residues of the PHGG(G/S)WGQ segment in the four peptide mimetics are shifted upfield (Fig. 3). The α protons of G10 of **L1**, **L2**, **C1**, and **C2** were also shifted significantly upfield. The same was observed for G18 of **L2** and **C2**. The present observation provides qualitative evidence for a non-extended conformation consistent with a β-turn at GWGQ.

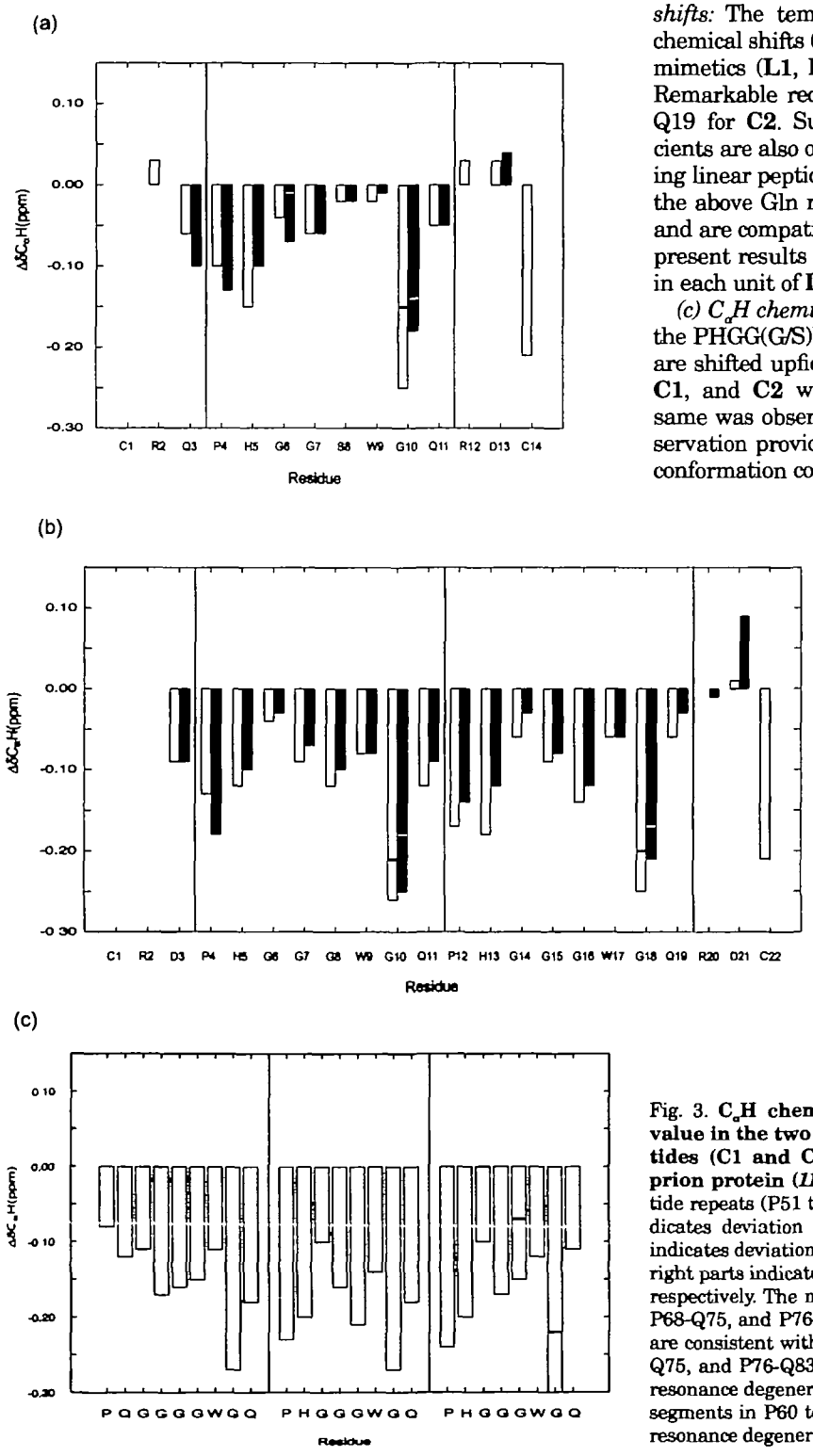

Fig. 3. **$C_\alpha H$ chemical shift deviation from the random coil value in the two linear peptides (L1 and L2), two cyclic peptides (C1 and C2), and the octapeptide repeats of human prion protein (*11*).** (a) **L1** and **C1**; (b) **L2** and **C2**; (c) the octapeptide repeats (P51 to Q91) of human prion protein. The white bar indicates deviation of the linear peptide (**L1** or **L2**), and gray bar indicates deviation of the cyclic peptide (**C1** or **C2**). In (c) the left and right parts indicate the P51-Q59 segment and the P84-Q91 segment, respectively. The middle part also indicates the segments P60-Q67, P68-Q75, and P76-Q83, of which the $C_\alpha H$ chemical shift deviations are consistent with each other. The GWG segment of P60-Q67, P68-Q75, and P76-Q83 could not be individually assigned due to other resonance degeneracies (*60*). Individual assignments of the QPHGG segments in P60 to Q91 could not be achieved because of extensive resonance degeneracy (*60*).

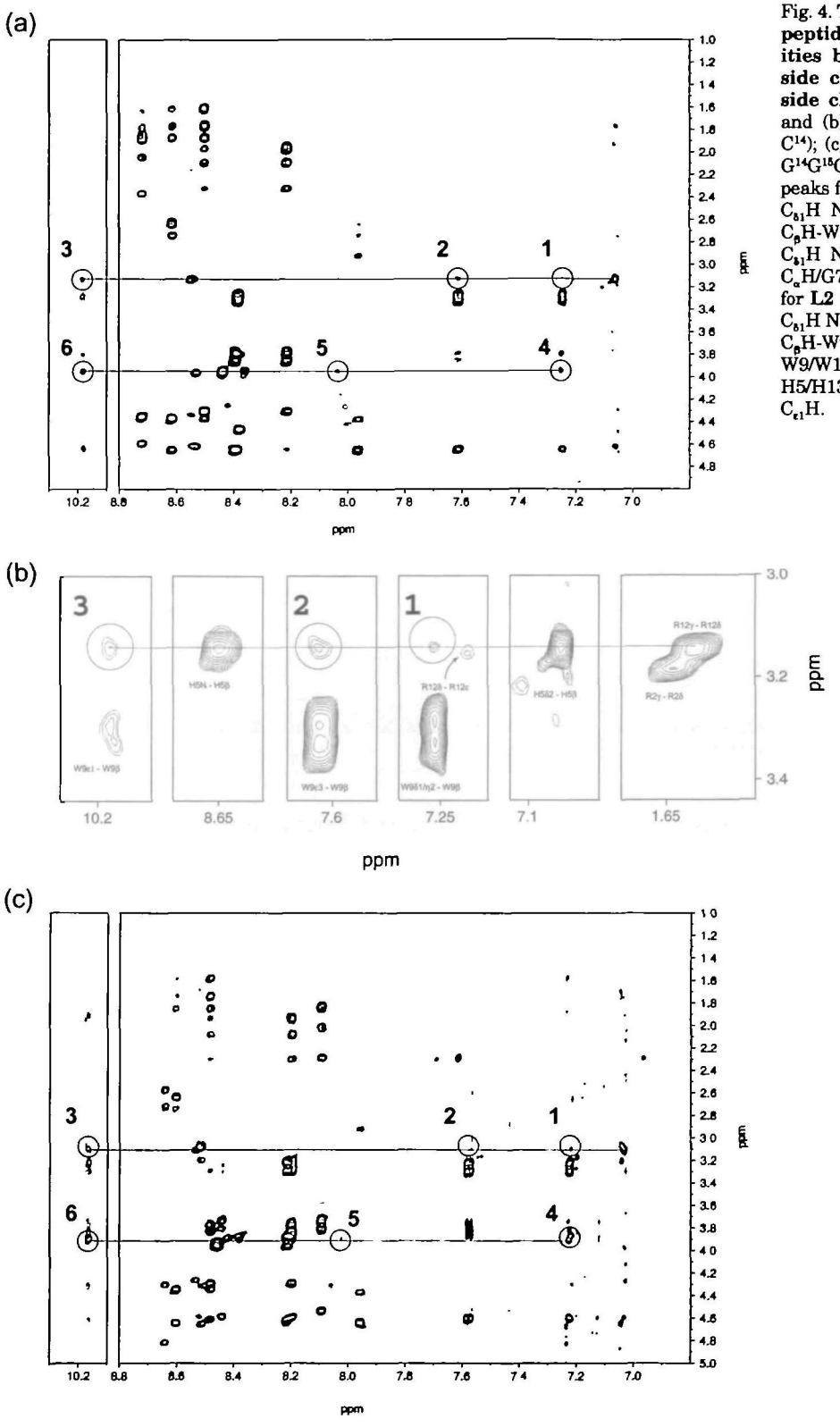

Fig. 4. **The NOESY spectra of the two linear peptides (L1 and L2) containing connectivities between the protons of tryptophan side chain and the β-proton of histidine side chain or the α-proton of glycine.** (a) and (b) **L1** ($C^1R^2Q^3P^4H^5G^6G^7S^8W^9G^{10}Q^{11}R^{12}D^{13}$-$C^{14}$); (c) **L2** ($C^1R^2D^3P^4H^5G^6G^7G^8W^9G^{10}Q^{11}P^{12}H^{13}$-$G^{14}G^{15}G^{16}W^{17}G^{18}Q^{19}R^{20}D^{21}C^{22}$). The circled cross-peaks for **L1** are as follows: **1**, H5 C_βH-W9 $C_{\zeta 2}$H/$C_{\delta 1}$H NOE; **2**, H5 C_βH-W9 $C_{\zeta 3}$H NOE; **3**, H5 C_βH-W9 $C_{\varepsilon 1}$H NOE; **4**, G6 C_αH/G7C_αH-W9 $C_{\zeta 2}$H/$C_{\delta 1}$H NOE; **5**, G6 C_αH/G7 C_αH-H5$C_{\varepsilon 1}$H; **6**, G6 C_αH/G7 C_αH-W9 $C_{\varepsilon 1}$H. The circled cross-peaks for **L2** are as follows: **1**, H5 C_βH-W9/W17 $C_{\zeta 2}$H/$C_{\delta 1}$H NOE; **2**, H5 C_βH-W9/W17 $C_{\zeta 3}$H NOE; **3**, H5 C_βH-W9/W17 $C_{\varepsilon 1}$H NOE; **4**, G7 C_αH/G15 C_αH-W9/W17 $C_{\zeta 2}$H/$C_{\delta 1}$H NOE; **5**, G7 C_αH/G15 C_αH-H5/H13 $C_{\varepsilon 1}$H; **6**, G7 C_αH/G15 C_αH-W9/W17 $C_{\varepsilon 1}$H.

Conformation of L1 Peptide—All distance constraints used for structure calculation are shown in Table II. Figure 6 shows superposition of 15 calculated structures of **L1** using distance-geometry and SA protocols with NMR-derived constraints. The ensemble displays a low RMSD for the segment P4-Q11 (Table III). The structure calculation indicates that the imidazole side chain of His5 is in close proximity to the aromatic ring of Trp9. Consequently, the HGGSW segment adopts a loop structure. The distance between the α protons of S8 and Q11 is less than 7 Å in the

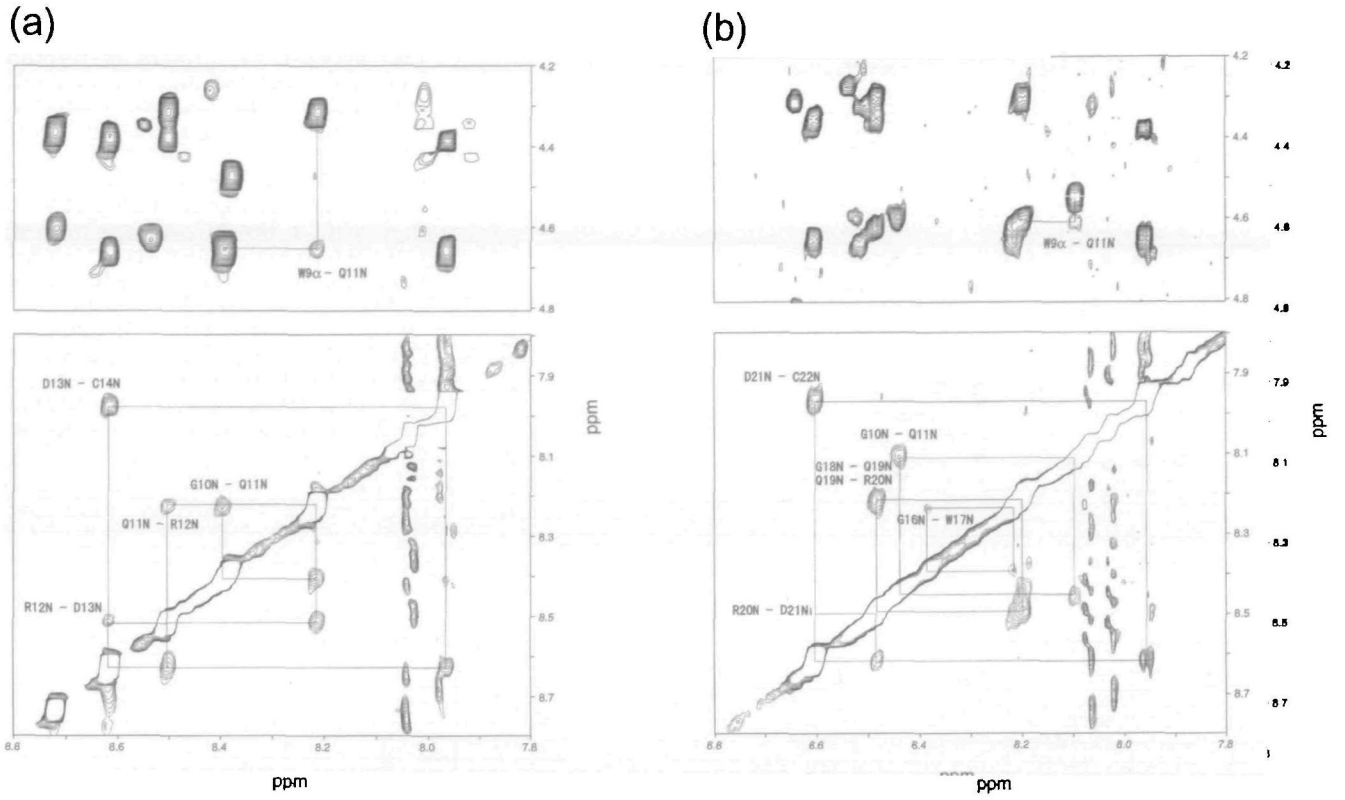

Fig. 5. **NH-NH and NH-C_αH regions of the NOESY spectra of the two linear peptides (L1 and L2).** (a) **L1** ($C^1R^2Q^3P^4H^5G^6G^7S^8$-$W^9G^{10}Q^{11}R^{12}D^{13}C^{14}$); (b) **L2** ($C^1R^2D^3P^4H^5G^6G^7G^8W^9G^{10}Q^{11}P^{12}H^{13}G^{14}G^{15}G^{16}W^{17}G^{18}Q^{19}R^{20}D^{21}C^{22}$).

15 calculated structures (*34*). The turn structure at the SWGQ segment is defined as a β-turn. Table II summarizes the statistics for the structures shown in Fig. 6.

DISCUSSION

*Structure of **L1** and **L2** Peptides*—The NOE data indicate that the β proton of His5 is in close proximity to the aromatic ring of Trp9 (Fig. 4). The structure calculation of **L1** indicates that the imidazole side chain of His5 is in close proximity to the aromatic ring of Trp9 (Fig. 6). Similar contacts (H5-W9 and H13-W17) are also suggested in both the first unit and the second unit of **L2**. The structure of **L1** indicates that the HGG(G/S)W and (G/S)WGQ segments adopt a loop structure and a β-turn, respectively (Fig. 6).

Many short linear peptides have been found to adopt preferentially defined structures in rapid equilibrium with extended-chain conformations of a random coil (*35, 36*). The NOE peaks are proportional to the inverse of internuclear distance to the sixth power (*37*), so that it is possible to detect transient structures that do not occupy a large population but have short inter-proton distance. Thus, it appears that there is uncertainty with regard to the population occupied by the defined structures as deduced from NOE data, due to the strong bias of this technique towards short distances. However, the ensemble of structure calculation indicates a low RMSD for P4-Q11 of **L1** (Table II). This result and the following observations suggest that the HGGGWGQ segment predominantly populates one conformation which may be in fast exchange with the random coil state.

As noted, circular dichroism spectra suggested the presence of an extended conformation with properties similar to polyproline II (*13*). At this stage we can not understand the difference between the CD and our NMR results.

*Structure of **C1** and **C2** Peptides*—Cyclic peptides have been used commonly to characterize turn structures (*14, 38*). In **C1** and **C2** peptides, the presence of a β-turn at GWGQ was suggested, as discussed later. However, the NMR data of **C1** and **C2** peptides did not suggest the close proximity of the imidazole side chain of His to the aromatic ring of Trp, which was observed in **L1** and **L2** peptides. This would be a result of the low peptide concentration used here, conformational restriction due to cyclization, or both.

Histidine–Tyrptophan Interaction in the PHGGGWGQ Repeats—A recent statistical survey of protein crystal structure has shown that the frequency of aromatic amino acids in proximity to histidine is higher than random. Many examples of such juxtaposition are found in the literature (*39–49*). A search through the Protein Data Bank (PDB) was made for the HGGGW sequence. A homologous sequence, HSGAY (residues 398–402) from cytolysin (*50*), was found to adopt a loop structure in which His (H398) is in proximity to Tyr (Y402).

The histidine-tryprophan/phenyalanine interaction has been mainly explained by cation-π interaction (*43, 44, 51, 52*). In barnase, Trp94 interacts strongly with the protonated form of His18 (*43*). At the pH value (pH = 6.6) used here, the solution contains half-protonated His, because the pK_a of the unpertubed His residue is 6.6 (*58*). Thus, we suggest that the histidine-tyrptophan interaction in the PHG-

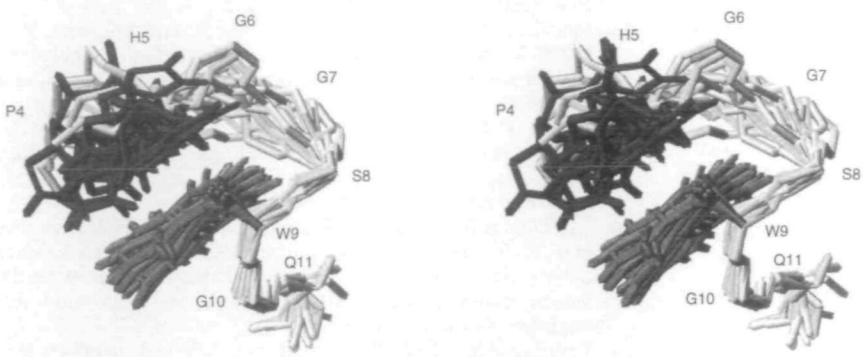

Fig. 6. **Three-dimensional structures of linear peptide L1.** Fifteen superimposed structures for $C^1R^2D^3P^4H^5G^6G^7G^8W^9G^{10}Q^{11}$-$R^{12}D^{13}C^{14}$ calculated with constraints derived from NMR experiments in aqueous solution. Only the segment P4-Q11 is displayed.

TABLE II. **NOE constraints used for the structure calculation of L1 peptide.**

Atom 1	Atom 2	Upper limits (Å)
R2 β	Q3 N	4.5
R2 γ	Q3 N	4.5
Q3 α	Q3 γ	3.5
Q3 N	Q3 β	5.0
Q3 N	Q3 γ	5.0
P4 β	H5 δ2	5.0
P4 β	H5 N	5.5
P4 γ	H5 δ2	5.5
H5 N	H5 β	4.5
H5 α	H5 δ2	5.0
H5 β	W9 ε1	5.5
H5 β	H5 δ2	4.5
H5 β	H5 ε1	5.5
H5 β	W9 ε3	4.5
G7 α	W9 ε1	5.5
W9 α	Q11 N	5.5
W9 ε1	G10 α	5.5
W9 ε1	Q11 α	5.5
W9 ε3	G10 α	4.5
W9 α	W9 ε1	5.5
W9 α	W9 ε3	4.5
W9 β	W9 ε1	5.0
G10 N	Q11 N	5.0
Q11 α	Q11 γ	3.5
Q11 N	Q11 β	4.5
Q11 N	Q11 γ	4.5
Q11 N	R12 N	5.0
Q11 β	R12 N	5.5
Q11 γ	R12 N	5.5
R12 N	R12 β	4.5
R12 N	R12 γ	4.5
R12 N	D13 N	5.0
R12 β	D13 N	5.0
R12 γ	D13 N	5.0
D13 N	D13 β	5.0
D13 N	C14 N	4.5
D13 β	C14 N	5.0
C14 N	C14 β	5.0

GGWGQ repeats is strengthened by the cation-π interaction.

Interestingly, the tryprophan is four residues distant from the histidine in the PHGGGWGQ repeats. It might be assumed that the HGGGW segment adopts an α-helix, since the spacing is consistent with that in an α-helix (*45*, *47*, *52*, *53*, *54*). However, glycine-rich segments do not preferentially form an α-helix. In addition to the H5-W9 NOEs, the medium-range NOEs between G7 and W9 of **L1** and be-tween G14 and W17 of **L2** are observed. Thus, the formation of an α-helix is unlikely. As indicated in Fig. 6, the HGGGW segment adopts a loop conformation.

TABLE III. **Structural statistics and rmsd for 15 structures of L1 peptide.**

Structural statistics	Value
Number of distance constraints	38
Intraresidual	17
Sequential	16
Medium	5
Number of dihedral-angle constraints	1
Average total energy (kcal/mol)	15.907±0.038
RMS deviations of the ensemble of structures on the average structure (Å)	
Backbone, residue 1–14	3.80±1.13
Heavy atom, residue 1–14	4.90±1.07
Backbone, residue 4–11	1.40±0.61
Heavy atom, residue 4–11	2.21±0.65

It is of interest to note the hexapeptide repeats, $(PHNPGY)_8$, of chicken prion protein (*55*). The disposition of the four-residue interval between histidine and tryprophan in the PHNPGY repeats is in agreement with the PHGGGWGQ repeats. Thus it is expected that PHNPGY may adopt a loop conformation similar to PHGGGWGQ.

β-Turn of (G/S)WGQ in the PHGGGWGQ Repeats—The secondary structure algorithm of Garnier *et al.* (*56*) indicates that GWGQ prefers β-turns (not shown). The present NMR data and the structure calculation of **L1** (Fig. 6) support this prediction. The NMR data including (i) remarkably reduced temperature coefficients of the amide proton chemical shifts of Gln at position 4 of β-turn, (ii) strong d_{NN} (3,4) NOE connectivities of Gly-Gln, $d_{\alpha N}$ (2,4) NOE connectivities of Trp-Gln, and (iii) very large $C_\alpha H$ chemical shift difference of Trp at position 2 and of Gly at position 3, all indicate a β-turn at GWGQ. In the structure of **L1**, the hydrophobic side chain of tryptophan is located on the turn part (Fig. 6). The upfield shift of the α proton of G10 (Gly at position 3) would be intensified by the ring-current shielding of the tryptophan aromatic moiety (Fig. 3). Thus, the tryptophan side chain seems to contribute to the stabilization of the turn structure at (G/S)WGQ. A search through the PDB was made for the (G/S)WGQ sequence. The GWGQ segment (residues 235–238) from folypolyglutamate synthetase was found to adopt a turn-like structure (*57*).

Interestingly, the temperature coefficient of the amide proton chemical shifts for Q11 and Q19 of **C2** is lower than those of **L2** (Table I). Thus, it is likely that cyclization of model peptides promotes stabilization of the turn structure at (G/S)WGQ.

The Structure of Tandem Repeats within Prion Pro-

teins—NMR studies of full-length PrP revealed that the N-terminus including the tandem repeats is highly flexible (*9–11*). However, it does not necessarily follow that the flexible tail does not form part of a stable secondary structure or tertiary folded structure. The present results suggest that the HGG(G/S)WGQ segment in the tandem repeats within prion proteins adopt the preferred structure found for the peptide mimetics.

The octapeptide repeat region has been reported to be the binding site of Cu(II) (*2*, *3*, *5–8*). The loop structure at HGG(G/S)W appears to facilitate copper binding to the PHGGGWGQ repeats.

CONCLUSION

The NMR data of the model peptides indicate that histidine at the *i*-th position is in close proximity to tryptophan at the *i*+4-th position, and (G/S)WGQ prefers a β-turn. Structure calculation for **L1** indicates that HGG(G/S)W and (G/S)WGQ adopt a loop structure and a β-turn, respectively. The present results suggest that the tandem repeats within prion proteins adopt such a preferred structure, which would play an important role in the function of prion protein.

REFERENCES

1. Prusiner, S.B. (1998) Prions. *Proc. Natl. Acad. Sci. USA* **95**, 13363–13383
2. Brown, D.R., Qin, K., Herms, J.W., Madlung, A., Manson, J., Strome, R., Fraser, P.E., Kruck, T., von Bohlen, A., Schulz-Schaeffer, W., Giese, A., Westaway, D., and Kretzschmar, H. (1997) The cellular prion protein binds copper *in vivo*. *Nature* **390**, 684–687
3. Stöckel, J., Safar, J., Wallace, A.C., Cohen, F.E., and Prusiner, S.B. (1998) Prion protein selectively binds copper (II) ions. *Biochemistry* **37**, 7185–7193
4. Viles, J.H., Cohen, F.E., Prusiner, S.B., Goodin, D.B., Wright, P.E., and Dyson, H.J. (1999) Copper binding to the prion protein: structural implications of four identical cooperative binding sites. *Proc. Natl. Acad. Sci. USA* **96**, 2042–2047
5. Hornshaw, M.P., McDermott, J.R., and Candy, J.M. (1995) Copper binding to the N-terminal tandem repeat regions of mammalian and avian prion protein. *Biochem. Biophys. Res. Commun.* **207**, 621–629
6. Hornshaw, M.P., McDermott, J.R., Candy, J.M., and Lakey, J.H. (1995) Copper binding to the N-terminal tandem repeat regions of mammalian and avian prion protein. *Biochem. Biophys. Res. Commun.* **214**, 993–999
7. Miura, T., Hori-i, A., and Takeuchi, H. (1996) Metal-dependent α-helix formation promoted by the glycine-rich octapeptide region of prion protein. *FEBS Lett.* **396**, 248–252
8. Miura, T., Hori-i, A., Motonami, H., and Takeuchi, H. (1999) Raman spectroscopic study on the copper (II) binding mode of prion octapeptide and its pH dependence. *Biochemistry* **38**, 11560–11569
9. Donne, D.G., Viles, J.H., Groth, D., Mehlhorn, I., James, T.L., Cohen, F.E., Prusiner, S.B., Wright P.E., and Dyson, H.J. (1997) Structure of the recombinant full-length hamster prion protein PrP(29-231): The N terminus is highly flexible. *Proc. Natl. Acad. Sci. USA* **94**, 13452–13457
10. Riek, R., Hornemann, S., Wider, G., Glockshuber, R., and Wüthrich, K. (1997) NMR characterization of the full-length recombinant murine prion protein, mPrP(23-231). *FEBS Lett.* **413**, 282–288
11. Zahn, R., Liu, A., Luhrs, T., Riek, R., von Schroetter, C., Lopez Garcia, F., Billeter, M., Calzolai, L., Wider, G., and Wüthrich, K. (2000) NMR solution structure of the human prion protein. *Proc. Natl. Acad. Sci. USA* **97**, 145–150
12. Morillas, M., Swietnicki, W., Gambetti, P., and Surewicz, W.K. (1999) Membrane environment alters the conformational structure of the recombinant human prion protein. *J. Biol. Chem.* **274**, 36859–36865
13. Smith, C.J., Drake, A.F., Banfield, B.A., Bloomberg, G.B., Palmer, M.S., Clarke, A.R., and Collinge, J. (1997) Conformational properties of the prion octa-repeat and hydrophobic sequences. *FEBS Lett.* **405**, 378–384
14. van Dijk, A.A., van Wijk, L.L., van Vliet, A., Haris, P., van Swieten, E., Tesser, G.I., and Robillard, G.T. (1997) Structure characterization of the central repetitive domain of high molecular weight gluten proteins. I. Model studies using cyclic and linear peptides. *Protein Sci.* **6**, 637–648
15. Brünger, A.T. (1992) *X-PLOR Mannual*, Yale University, New Haven, CT
16. Nilges, M., Kuszewski, J., and Brünger, A.T. (1991) *Computational Aspects of the Study of Biological Macromolecules by NMR*, Plenum Press, New York
17. Kuszewski, J., Nilges, M., and Brünger, A.T. (1992) Sampling and efficiency of metric matrix distance geometry: a novel partial metrization algorithm. *J. Biomol. NMR* **2**, 33–56
18. Nilges, M., Clore, G.M., and Gronenborn, A.M. (1988) Determination of three-dimensional structures of proteins from interproton distance data by dynamical simulated annealing from a random array of atoms. Circumventing problems associated with folding. *FEBS Lett.* **229**, 317–324
19. Merutka, G., Dyson, H.J., and Wright, P.E. (1995) Random coil ^{1}H chemical shifts obtained as a function of temperature and trifluoroethanol concentration for the peptide series GGXGG. *J. Biomol. NMR* **5**, 14–24
20. Wishart, D.S., Bigam, C.G., Holm, A., Hodges, R.S., and Sykes, B.D. (1995) ^{1}H, ^{13}C and ^{15}N random coil NMR chemical shifts of the common amino acids. I. Investigations of nearest-neighbor effects. *J. Biomol. NMR* **5**, 67–81
21. Schulz, G.E. and Schirmer, R.H. (1979) *Principles of Protein Structure*, Springer-Verlag, New York
22. Huber, R. and Steigemann, W. (1984) Two cis-Pro's in the Bence-Jones protein Rei and the cis-Pro-turn. *FEBS Lett.* **48**, 235–237
23. Grawthwohl C. and Wütrich, K. (1976) The X-Pro peptide bond as an nmr probe for conformational studies of flexible linear peptides. *Biopolymers* **15**, 2025–2041
24. Dyson, H.J., Rance, M., Houghten, R.A., Lerner, R.A., and Wright, P.E. (1988) Folding of immunogenic peptide fragments of proteins in water solution. I. Sequence requirements for the formation of a reverse turn. *J. Mol. Biol.* **201**, 161–200
25. de Alba, E., Jimnez, M.A., and Rico, M. (1997) Turn residue sequence determines β-hairpin conformation in designed peptides. *J. Am. Chem. Soc.* **119**, 175–183
26. Johnson, W.C., Jr, Pagano, T.G., Basson, C.T., Madri, J.A., Gooley, P., and Armitage, I.M. (1993) Biologically active Arg-Gly-Asp oligopeptides assume a type II β-turn in solution. *Biochemistry* **32**, 268–273
27. Ramirez-Alvarado, M., Blanco, F.J., Niemann, H., and Serrano, L. (1997) Role of β-turn residues in β-hairpin formation and stability in designed peptides. *J. Mol. Biol.* **273**, 898–912
28. Otter, A., Scott, P.G., Liu, X.H., and Kotovych, G. (1989) A ^{1}H and ^{13}C NMR study on the role of salt-bridges in the formation of a type I β-turn in *N*-acetyl-L-Asp-L-Glu-L-Lys-L-Ser-NH_2. *J. Biomol. Struct. Dynam.* **7**, 455–476
29. Xu, G. and Evans, J.S. (1999) Model peptide studies of sequence repeats derived from the intracrystalline biomineralization protein, SM50. I. GVGGR and GMGGQ repeats. *Biopolymers* **49**, 303–312
30. Maynard, A.J., Sharman, G.J., and Searle, M.S (1998) Origin of β-hairpin stability in solution: structural and thermodynamic analysis of the folding of a model peptide supports hydrophobic stabilization in water. *J. Am. Chem. Soc.* **120**, 1996–2007
31. Haque, T.S. and Gellman, S.H. (1997) Insights on β-hairpin stability in aqueous solution from peptides with enforced type I′ and type II′ β-turns. *J. Am. Chem. Soc.* **119**, 2303–2304

32. Kieffer, B., Mer, G., Mann, A., and Lefevre, J.F. (1993) Structural studies of two antiaggregant RGDW peptides by ^{1}H and ^{13}C NMR. *Int. J. Pept. Protein Res.* **44**, 70–79
33. Morelli, M.A., DeBiasi, M., DeStradis, A., and Tamburro, A.M. (1993) An aggregating elastin-like pentapeptide. *J. Biomol. Struct. Dyn.* **11**, 181–190
34. Wilmot, C.M. and Thornton, J.M (1988) Analysis and prediction of the different types of β-turn in proteins. *J. Mol. Biol.* **203**, 221–232
35. Dyson, H.J., Merutka, G., Waltho, J.P., Lerner, R.A., and Wright, P.E. (1992) Folding of peptide fragments comprising the complete sequence of proteins. Models for initiation of protein folding. I. Myohemerythrin. *J. Mol. Biol.* **226**, 795–817
36. Chang, D.-K., Chien, W.-J., and Cheng, S.-F. (1997) The FLG motif in the N-terminal region of glucoprotein 41 of human immunodeficiency virus type 1 adopts a type-I β-turn in aqueous solution and serves as the initiation site for helix formation. *Eur. J. Biochem.* **247**, 896–905
37. Abragam, A. (1961) *The Principles of Nuclear Magnetism*, Oxford University Press, Oxford
38. Perczel, A. and Hollósi, M. (1996) Turns in *Circular Dichroism and the Conformational Analysis of Biomolecules* (Fasman, G.D., ed.) pp. 285–380, Plenum Press, New York
39. Anglister, J. and Zilber, B. (1990) Antibodies against a peptide of cholera toxin differing in cross-reactivity with the toxin differ in their specific interactions with the peptide as observed by ^{1}H NMR spectroscopy. *Biochemistry* **29**, 921–928
40. Kochoyan, M., Keutmann, H.T., and Weiss, M.A. (1991) Alternating zinc fingers in the human male associated protein ZFY: refinement of the NMR structure of an even finger by selective deuterium labeling and implications for DNA recognition. *Biochemistry* **30**, 7063–7072
41. Wery, J.P., Schevitz, R.W., Clawson, D.K., Bobbitt, J.L., Dow, E.R., Gamboak, G., Goodson, T. Jr., Hermann, R.B., Kramer, R.M., McClure, D.B., Mihelich, E.D., Putman, J.E., Sharp, J.D., Stark, D.H., Teater, C., Warrick, M.W., and Jones, N.D. (1991) Structure of recombinant human rheumatoid arthritic synovial fluid phospholipase A2 at 2.2 Å resolution. *Nature* **352**, 79–82
42. Ito, N., Phillips, S.E., Stevens, C., Ogel, Z.B., McPherson, M.J., Keen, J.N., Yadav, K.D., and Knowles, P.F. (1991) Novel thioether bond revealed by a 1.7 Å crystal structure of galactose oxidase. *Nature* **350**, 87–90
43. Loewenthal, R., Sancho, J., and Fersht, A.R. (1992) Histidine-aromatic interactions in barnase. elevation of histidine pK_a and contribution to protein stability. *J. Mol. Biol.* **224**, 759–770
44. Fernandez-Recio, J., Romero, A., and Sancho, J. (1999) Energetics of a hydrogen bond (charged and neutral) and of a cation-π interaction in apoflavodoxin. *J. Mol. Biol.* **290**, 319–330
45. Wilmot, C.M., Hajdu, J., McPherson, M.J., Knowles, P.F., and Phillips, S.E. (1999) Visualization of dioxygen bound to copper during enzyme catalysis. *Science* **286**, 1724–1728
46. Demarest, S.J., Fairman, R., and Raleigh, D.P. (1998) Peptide models of local and long-range interactions in the molten globule state of human α-lactalbumin. *J. Mol. Biol.* **283**, 279–291
47. Demarest, S.J., Hua, Y., and Raleigh, D.P., (1999) Local interactions drive the formation of nonnative structure in the denatured state of human α-lactalbumin: a high resolution structural characterization of a peptide model in aqueous solution. *Biochemistry* **38**, 7380–7387
48. Smith, L.J., Alexandrescu, A.T., Pitkeathly, M., and Dobson, C.M. (1994) Solution structure of a peptide fragment of human α-lactalbumin in trifluoroethanol: a model for local structure in the molten globule. *Structure* **2**, 703–712
49. Gaskell, A., Crennell, S., and Taylor, G. (1995) The three domains of a bacterial sialidase: a beta-propeller, an immunoglobulin module and a galactose-binding jelly-roll. *Structure* **3**, 1197–1205
50. Rossjohn, J., Feil, S.C., McKinstry, W.J., Tweten, R.K., and Parker, M.W. (1997) Structure of a cholesterol-binding, thiol-activated cytolysin and a model of its membrane form. *Cell* **89**, 685–692
51. Dougherty, D.A. (1996) Cation-pi interactions in chemistry and biology: a new view of benzene, Phe, Tyr, and Trp. *Science* **271**, 163–168
52. Fernandez-Recio, J., Vazquez, A., Civera, C., Sevilla, P., and Sancho, J. (1997) The tryptophan/histidine interaction in α-helices. *J. Mol. Biol.* **267**, 184–197
53. Shoemaker, K.R., Fairman, R., Schultz, D.A., Robertson, A.D., York, E.J., Stewart, J.M., and Baldwin, R.L. (1990) Side-chain interactions in the C-peptide helix: Phe8...His12^{+}. *Biopolymers* **29**, 1–11
54. Wlodawer, A., Svensson, L.A., Sjolin, L., and Gilliland, G.L. (1988) Structure of phosphate-free ribonuclease A refined at 1.26 Å. *Biochemistry* **27**, 2705–2717
55. Gabriel, J.M., Oesch, B., Kretzschmar, H., Scott, M., and Prusiner, S.B. (1992) Molecular cloning of a candidate chicken prion protein. *Proc. Natl. Acad. Sci. USA* **89**, 9097–9101
56. Garnier, J., Osguthorpe, D.J., and Robson, B. (1978) Analysis of the acccuracy and implications of simple methods for predicting the secondary structure of globular proteins. *J. Mol. Biol.* **120**, 97–120
57. Sun, X., Bognar, A.L., Baker, E.N., and Smith, C.A. (1998). Structural homologies with ATP- and folate-binding enzymes in the crystal structure of folylpolyglutamate synthetase. *Proc. Natl. Acad. Sci. USA* **95**, 6647–6652
58. McNutt, M., Mullins L.S., Raushel, F.M., and Pace, C.N. (1990) Contribution of histidine residues to the conformational stability of ribonuclease T1 and mutant Glu-58—Ala. *Biochemistry* **29**, 7572–7576
59. Kretzschmar, H.A., Stowring, L.E., Westaway, D., Stubblebine, W.H., Prusiner, S.B., and Dearmond, S.J. (1986) Molecular cloning of a human prion protein cDNA. *DNA* **5**, 315–324
60. Liu, A., Riek, R., Wider, G., von Schroetter, C., Zahn, R., and Wuthrich, K. (2000) NMR experiments for resonance assignments of ^{13}C, ^{15}N doubly-labeled flexible polypeptides: application to the human prion protein hPrP(23-230). *J. Biomol. NMR* **16**, 127–138